

Impact of local and remote winds on the shelf circulation off the central west coast of India

P. Amol^{a,*}, V. Vijith^b, V. Fernando^c, P. Pednekar^c, J. Singh^c

^aCSIR-National Institute of Oceanography, Regional Centre, Visakhapatnam, India

^bSchool of Marine Sciences, Cochin University of Science and Technology, Ernakulam, India

^cCSIR-National Institute of Oceanography, Goa, India

*Corresponding author Email address:

amol@nio.org (P. Amol) URL: www.nio.org (P. Amol)

Abstract

A linear coastal-trapped-wave (CTW) model is used to examine the effects of large-scale winds, with time scale ranging from a few days to a few weeks, on the West India Coastal Current (WICC), particularly on the shelf off the central west coast of India. We show that unlike the seasonal cycle of WICC, which is primarily forced by the winds along the east coast of India, the high-frequency WICC is mostly driven by the west-coast winds. Nevertheless, the influence of winds as far as Sri Lanka and east coast of India cannot be neglected. Simple numerical experiments with the CTW model show that the strong current observed at Goa (15° N) compared to Bhatkal (13° N) and Jaigarh (17° N) is due to two factors: 1) the superposition of local and remote CTWs, and 2) the widening of shelf width north of Goa, which decreases the amplitude of the currents poleward of Goa. If the local winds are weak, the amplitude of current decreases poleward due to friction, and the current at the south lead the north. We also note that the observed phase difference between sea level and alongshore current at Goa could be attributed to the propagation of remotely-forced higher-order modes of CTWs.

Keywords: Trapped waves, Current observations, Shelf dynamics, Wind-driven currents, West India Coastal Current, Arabian Sea

1. Introduction

Though the effect of remote forcing is ubiquitous to the circulation around the world, the West India Coastal Current (WICC) is one of the current systems where this effect is perhaps more palpably observed. The alongshore winds off the west coast of India are uni-directional throughout the year, whereas the alongshore currents reverse direction once a year. Model studies (McCreary et al., 1993; Shankar & Shetye, 1997; Shankar et al., 2002) have shown that this switch in the direction of the slope WICC is primarily caused due to the strong seasonal cycle of alongshore winds along the east coast of India. These east-coast winds generate Kelvin waves, which travel equatorward along the east coast of India, turn around Sri Lanka, and further propagate poleward along the west coast of India. Depending on the season of the year, the annual cycle of the east-coast winds changes the WICC from upwelling favourable (during summer monsoon) to downwelling favourable (during winter monsoon) and vice versa. A detailed description of the observed circulation and the theoretical background of currents along the coast of India can be found in Amol et al. (2014) and Mukherjee et al. (2014).

On the shelf, however, the dynamics differ. The remote information, at sub-inertial time scales, is carried by a special class of waves known as the coastal-trapped waves (CTWs) — generated as a consequence of a change in topography and stratification. The first evidence, for such waves along the west coast of India, was shown by Shetye et al. (2008) using a set of current-meter measurements off the central west coast of India. They had noted that at periods greater than 10 days, the local winds were unidirectional, but the currents reversed direction. The source of this reversal was traced to southern tip of India where the winds reversed direction along with the currents. For period shorter than 10 days, the local winds and currents were highly correlated, and the winds lead the currents by ~ 1 day. These measurements were carried out at a shallow depth of about 20–30 m for a period of one month.

The evidence was further corroborated by Amol et al. (2012) using a set of acoustic Doppler current profilers (ADCPs) deployed near the shelf-edge. The data showed signatures for poleward propagating CTWs at periods as short as 4 days. Amol et al. (2012) noted that such propagating events were observed when the local winds were weak and remote winds were strong. They confirmed the presence of these waves by separating the local and remote response using a linear CTW model (Brink & Chapman, 1987).

Though the CTW theory was successfully applied along the west coast of India, several questions pertaining to the observed features of the shelf WICC still remained unanswered. For example,

observations from direct current measurements suggest that remote forcing is important for the shelf-edge circulation at periods shorter than 10 days (Amol et al., 2012) but not for the nearshore circulation (Shetye et al., 2008). Are the high-frequency CTWs damped near the coast and not farther offshore? Also, the free-wave-propagation events identified by Amol et al. (2012) were evident only on certain occasions. The phase speed varied and the amplitude of CTWs did not necessarily decrease poleward owing to friction. What causes such differences in phase and magnitude?

The success of a simple linear shelf theory (Brink, 1982b,a; Clarke & Van Gorder, 1986) applied along the west coast of India (Amol et al., 2012) has enabled us to further explore the influence of CTWs on the shelf circulation. In this manuscript, we extend the CTW theory to the inner shelf circulation and show evidence for the high-frequency CTWs from direct current measurements. We further show that the high-frequency variability associated with the shelf WICC, particularly off the central west coast of India, is primarily forced by west coast winds. The linearity principle of the model further allows us to explain several observed features of the shelf WICC using superposition of local and remote CTWs. For instance, the current off the central west coast of India amplifies polewards due to the addition of remote waves but weakens further north of Goa due to the widening or the sudden change in the shelf profile. Similarly, the amplitude and phase difference observed between the CTWs at two stations (Amol et al., 2012) could be explained by the type of wind forcing (propagating or stationary winds) present over the region.

The manuscript is organised as follows. In Section 2, we present the data sets and model equations. The model's ability to reproduce some of the important features of shelf WICC is presented in Section 3. The relative importance of local and remote forcing on the shelf WICC and the evidence for CTWs from the nearshore current meters are also shown in this section. In Section 4, we show a series of model runs using idealised wind forcing. These simulations are used to explain the observed amplitude and phase difference between currents at each mooring location. It is further shown that remote forcing could generate a possible lead/lag between current and sea level (also, current and wind). We also show how a change in bathymetry along the west coast could influence the magnitude of currents. This is followed by a brief discussion on the results of the study (Section 5).

2. Data and Methods

2.1. Observations

The currents, sea level, and wind data were collected off the central west coast of India (see Figure 1 and Table 1 for details). The current measurements were carried out at three locations, Bhatkal (~13° N); Goa (~15° N); and Jaigarh (~17° N), separated by a distance of 150–200 km. The

Teledyne RD Instruments ADCPs were used to collect current data near the shelf-edge at ~100 m. The data from six-month ADCPs were reported earlier by Amol et al. (2012). The data were collected from March to October 2008. The standard deviation of velocity error for the ADCP is less than 1.55 cm s^{-1} . The top 10% of the data were removed owing to surface backscatters. The ADCP bin size is 4 m, and the data were collected at every 15-minute interval. We have also included data from an additional one-year ADCP deployed near the shelf-edge at Goa during the year 2011–2012. The ADCP frequency and water-column depth are different from the six-month ADCPs mentioned before (Table 1).

Aanderaa RCM9 self-recording current meters were used to measure the nearshore currents at 20–35 m water column depth. The nearshore currents were measured for one month. The accuracy of RCM9 is $\pm 2\%$ for the speed, and ± 10 degree for the direction. The measurements were made at 10-minute interval.

The wind data were obtained from an anemometer, which was located on the rooftop of the CSIR-National Institute of Oceanography, Goa, and the QuikSCAT (ASCAT for 2011 data) scatterometer. The data from QuikSCAT have shown significant correlation with the anemometer data at Goa (Aparna et al., 2005). The winds speed and direction were decomposed and rotated following the coast angle to obtain the alongshore component. The sea level was measured using a Valeport tide gauge, which was deployed near the mouth of the Mandovi Estuary located at Goa. The accuracy of the tide gauge is $\pm 0.005 \text{ m}$ (0.1% of the range) and the data is measured at every 5-minute interval. The sea level barometric pressure correction was made using atmospheric pressure data from European Centre For Medium-Range Weather Forecasts (ECMWF) (Dee et al., 2011).

The current and sea level were detided using Tidal Analysis Software Kit (TASK) software (Bell et al., 1998). The TASK software uses harmonic analysis to separate the tidal constituents from the currents. The residual components were rotated, by minimising the cross-shore component, to compute the alongshore currents. Small data gaps, typically lasting a few days, were filled following the procedure by Johnson et al. (2007). The data were filtered using a 3rd-order Butterworth filter.

2.2. Model

We have used a linear CTW model with friction added in form of a small parameter. The stratification and friction parameters though constant are allowed to vary slowly along the coast. Details of the model may be found in earlier works on CTW by Brink (1982b,a), and Clarke & Van Gorder (1986). The model settings are same as Amol et al. (2012).

The pressure here is expressed in terms of free wave modes,

$$P = \sum F_n(x,z)\phi_n(y,t), \quad (1)$$

which obeys

$$F_{nxx} + f^2(F_{nz}N^2)z = 0. \quad (2)$$

With appropriate boundary conditions, the equation for ϕ_n for a forced problem is

$$c_n^{-1}\phi_{nt} + \phi_{ny} + a_{nm}\phi_n = b_n\tau(y,t) - \sum_{i \neq n}^{i=1} a_{ni}\phi_n \quad (3)$$

where a_{nm} and b_n are the frictional and wind coupling coefficients, respectively. The subscripts n and m are the mode numbers. τ is wind stress. Solutions for uncoupled modes ($n \neq m$) are obtained by neglecting the last term in the Equation 3. Earlier studies have shown that this coupling term has minor effects on the calculation of alongshore currents and the hindcast remained almost unchanged (Church et al., 1986; Chapman, 1987). For most cases, we restrict our analysis to the first mode. In Section 4.4, we briefly discuss the influence of higher-order modes. Equation 3 is a first-order wave equation and can be solved using method of characteristics to obtain

$$\phi(y,t) = \phi(0, t - \int_0^y c_n^{-1} d\xi) \exp(-\int_0^y a_{nn} d\xi) + \int_0^y b_n(\xi) \tau_0^y(\xi, t - \int_\xi^y c_n^{-1} d\xi') \exp(-\int_\xi^y a_{nn} d\xi') d\xi. \quad (4)$$

$y = 0$ is the starting point of the integration, which is set at the southern tip of India (Figure 1). The first term on the right-hand side (RHS) of Equation 4 is set to zero. In making this assumption, we have neglected the effect of winds south of the southern tip of India; i.e. any wave that is generated farther ‘upstream’ (for example, off the coast of Sri Lanka or the east coast of India) is assumed to be damped before reaching the model southern boundary. For integration, the model domain is divided into nine one-degree-latitude blocks (Figure 1). To separate the locally forced current from the total current, the integral was calculated over the local block of the particular location. For example, to estimate the locally forced current at 15.5° N, the limits of the integral were taken to be 14.5° N and 15.5° . For each block, the bathymetry and stratification inputs are set to climatological values, and the wind stress is provided from QuikSCAT/ASCAT. The cross-shelf topography are prescribed from 2-minute bathymetry of Sindhu et al. (2007). The profiles are smoothed using a 7-point

triangular filter. The temperature and salinity values for calculating the Brunt-Väisälä frequency (N) are from one-degree climatology of Chatterjee et al. (2012). The values are picked from 1500 m isobath off-coast and are averaged over time based on the length of the data. The eigenfunctions (F_n), the eigenvalues (c_n), the wind coefficient (b_n), and friction-coupling (a_{nn}) coefficient are obtained from the code developed by Brink & Chapman (1987). The term a_{nn} consists of a linear bottom friction coefficient ($r(x)$), which is kept constant (0.02 cm s^{-1}). The model parameters for the first mode is shown in Table 2. The alongshore velocity was computed assuming a geostrophic balance:

$$v = \frac{P_x}{\rho_0 f}. \quad (5)$$

3. Hindcasting

3.1. Shelf-edge circulation

Comparison of CTW model solutions, for the first mode, with a one-year continuous current record near the shelf-edge off Goa shows a poor simulation of currents, especially during the winter monsoon (Figure 2a). The observed current is poleward from January to mid-May, whereas the modelled current is equatorward. Observations show that the winds are equatorward along the west coast of India during the winter monsoon, leading to an equatorward flow in the CTW model. The inability of the model to capture the seasonal reversal of currents suggests that the influence of wind forcing from the east coast of India, Gulf of Mannar, and Sri Lankan coast (which is not included in the model) is important at seasonal time scales. On the slope, studies have shown that this poleward flow is strongly influenced by winds along the east coast of India and our results suggest a similar influence on the shelf. When a 5–30-day band-pass filter is applied to filter out the seasonal cycle and pick the high-frequency variability, periods ranging from a few days to a few weeks, the model shows considerable improvement in the simulation of currents (Figure 2b). The correlation between the observed and modelled current is 0.54 and the root-mean-square error is 4.5 cm s^{-1} . The better simulation of currents in this frequency band suggests that unlike the low-frequency currents, the high-frequency alongshore currents are primarily driven by winds along the west coast of India. Nevertheless there are several occasions on which there is a mismatch between the observed and the modelled current.

3.2. Nearshore circulation

What happens nearer the shore? An earlier study using a one-month-long current-meter record from

the nearshore (depth 10–30 m) waters off Goa (Shetye et al., 2008) during March–April 2003 had shown that the current was largely locally forced at periods shorter than 10 days, but remote forcing from southwest coast of India dominated at periods of the order of 12–15 days. A similar set of current-meter data from the Goa coastal regime during March–April 2008 show distinctly different results. The high-frequency currents during 2008 are not correlated with high-frequency winds, especially in April, when the winds are stronger than in March (Figure 3a). This lack of correlation indicates that remote forcing is present even at periods lower than 10 days, which is contrary to the observations made during 2003. In contrast, the low-passed currents are in phase with the winds (Figure 3b) and seem to be locally forced.

Comparison with currents at Bhatkal (southern mooring) and Jaigarh (northern mooring) shows propagation events (Figure 4a,b) in both bands: 3–5 day and 10–30 day. A propagation event is identified when the current at the southern location leads the current at northern location, and such an event can therefore be linked to a poleward-travelling CTW. [In the absence of local winds, these waves are considered to be free waves that travel with a theoretical phase speed (c_n).] Note that when a propagation event is observed, the amplitude of the current decreases poleward, and during this time, the winds are weak at Goa (Figure 3c). The propagation is also observed in the shelf-edge currents for the 4-day period, but the shelf-edge currents lag the nearshore currents (Figure 4c,d). The amplitude of the shelf-edge currents do not decrease poleward, particularly from 29 March to 09 April, and are strongest at Goa. In the 10–30-day band, the propagation event is seen only when the currents are equatorward from 01 to 09 April. A similar phase difference between the shelf-edge and the nearshore currents is observed in this band. The magnitude of currents for both bands is seen to decrease offshore.

Propagation events for the 4-day and 12-day waves were shown earlier by Amol et al. (2012) over a longer record from the ADCP data on the shelf-edge (Moorings A2, A3, and A4 in Table 1). The propagation speeds calculated from these events were comparable to the theoretical first-mode phase speed, with the observed speed on an average being $0.3\text{--}0.4\text{ ms}^{-1}$ lower than the theoretical values (Amol, 2014).

We compared the CTW model results with the nearshore current-meter record at Goa. As the AWS wind data are not available all along the coast, we used QuikSCAT winds to force the model (Figure 3c). The low temporal resolution of QuikSCAT wind, which has a repeat interval of ~ 4 days, allows us to resolve only the low-frequency variability of the current (Figure 3d). The model is able to capture the strong reversal in the 10-day low-passed current from mid-March to April. Though the

local winds are in phase during this time, their contribution to the total current is very weak. The current is mostly driven by winds south of the mooring location. The wind contribution from the 7° N– 12° N block is stronger when the currents are poleward (during the last week of March). During the beginning of the record, the current is poleward and the model current remains equatorward. However, the winds are equatorward all along the west coast, suggesting that the current may be influenced by winds outside the model domain.

Maps of QuikSCAT meridional winds in north Indian Ocean (Figure 6) show strong winds outside the model domain, especially in Gulf of Mannar (see Figure 1 for location), off the coast of Sri Lanka, and off east coast of India. The winds in these region would modify the amplitude and phase of the modelled current.

On the shelf-edge, the Goa current is in opposite direction to the currents at Bhatkal and Jaigarh from March 9 to March 31 (Figure 4d). This local reversal in current at Goa is not picked by the CTW model (Figure 5). The model, nevertheless, shows an offshore decrease in amplitude consistent with the observations.

4. Model Experiments

To understand the dynamics of shelf WICC, we carried out CTW-model experiments with idealised wind forcing. The aim of these experiments is to explain, particularly, the observed phase and magnitude difference between current at different stations, current and wind, and current and sea level. We begin each experiment by showing a set of observations and use solutions from the model to explain the identified feature. In the first three experiments (Section 4.1–4.3) the model is run with different wind forcing — stationary, remote, and propagating — and only the effect of first mode is considered here. The influence of higher-order modes on the CTW solutions is presented in Section 4.4. The results from the model, unless stated otherwise, are shown at the current-meter locations (30 m isobath). As with the previous runs, the topography and stratification are allowed to vary with latitude.

4.1. Experiment 1: Stationary wind forcing

The sub-inertial alongshore currents from the six-month ADCPs show strong currents at Goa on the shelf compared to the currents at Bhatkal and Jaigarh (Figure 7). When Amol et al. (2012) filtered these currents along with the winds to pick the 12-day period, they observed a scenario where both wind and current were near-coherent along the central west coast of India. In Figure 8a–c (redrawn from Amol et al. (2012)), the winds and currents after applying a 10–14 day band-pass filter are seen to be near-coherent from 29 May to 9 June. The magnitude of winds at all three locations is similar,

but the current is strongest at Goa (15° N) and weakest at Jaigarh (17° N).

In order to explain this difference in current magnitude at different location, we force the model with spatially-uniform stationary winds and show that such winds amplifies the current polewards, but the change in bathymetry north of Goa negates this effect of the wind and weakens the current at Jaigarh.

We assume wind-forcing of the form

$$\tau = A \sin(\omega t). \quad (6)$$

Here, τ is the wind stress, A is the amplitude of the wind forcing (2 dyn cm⁻²), and ω is the frequency (0.25 and 0.1 day⁻¹). The model generates near-coherent currents (a small phase difference is seen between the stations) all along the central west coast of India (Figure 9a,b). The current was strongest at Goa for the 10-day period wind forcing (Figure 9b), but not for the 4-day-period wind forcing (Figure 9a). For both the periods, the locally-driven current at Bhatkal and Goa had similar magnitudes (Figure 9c,d). The magnitude of the currents at Goa is larger owing to an additional block included in the CTW calculations. That is, as the wave progress poleward, the number of blocks increases, and so does the contribution from the remote winds at the local station. Yet, the weakest current is observed at Jaigarh, which is the northernmost mooring. In this case, the increase in shelf width at Jaigarh modifies the eigenfunction (F_n) and the wind-coupling coefficient (b_n), which in turn decreases the magnitude of the local current. On the shelf, the eigenfunction is weaker at Jaigarh compared to Goa and Bhatkal (Figure 10), and the wind-coupling coefficient decreases from Bhatkal to Jaigarh (Table 2).

For the 4-day forcing, the drop in magnitude of the current at Goa is due to the superposition of remote waves with local waves that are not in phase. For example, a wave propagating (with an average first mode speed of 3 m s⁻¹) from the southern tip of India would take approximately 2.5 days to reach Goa. Therefore, when the remote waves from the southern tip of India reach Goa, they would be opposite phase to the locally generated waves, thereby decreasing the current amplitude. Strong currents at Goa compared to Bhatkal and Jaigarh for a 4–5 day period wave would imply that the currents are forced by winds north of 10° N. Winds south of 10° N would generate remote waves that are out of phase with the local waves, and their superposition would weaken the amplitude of the current at Goa. Winds south of the southern tip of India (i.e., from the Gulf of Mannar and beyond) would have negligible influence on the currents along the central west coast of India as the 4–5 day period becomes supra-inertial near the Indian southern tip, in turn inhibiting the generation of CTWs.

This increase in amplitude as the wave propagates poleward could also be explained in context of a frictionless solution for a barotropic shelf waves obtained by Gill & Schumann (1974). For the same wind forcing, the solution for ϕ_n could be written as $\frac{2c_n b_n A}{\omega f} \sin(\frac{\omega y}{2c_n}) \sin(\omega(t - \frac{y}{2c_n}))$. When the phase speed is fixed, the amplitude of the current is dependent on the frequency and varies sinusoidally with distance. For a wind forcing that originates at the southern tip of India, the amplitude of the 4-day wave drops before reaching Goa, but not that of the 10-day wave.

When the model is forced with QuikSCAT wind, it is able to capture a similar difference in magnitude (Figure 8d). However, the magnitude of Jaigarh current does not drop sharply as seen in the observations, and there is a small phase difference between the observed and modelled current. Amol et al. (2012) attributed this phase difference, which is of the order of a day, to the 3-day averaging of the QuikSCAT wind.

The strong currents at Goa on the shelf (Figure 7) also suggests a similar influence of bathymetry on the modulation of the current amplitude at other frequency bands. The currents from the slope moorings measured during the same time did not show any amplification of currents at Goa (see Figure 2 of Amol et al. (2012)). The shelf and slope moorings were separated by a distance of ~50 km only.

We also note here that in the beginning of the record (Figure 8b), from 17 to 26 May, the winds are weaker but still coherent. The currents, however, show a distinct difference in phase (Figure 8c). The Goa current leads the other two stations by a day or two. The model is unable to capture this response in phase, and we presume this could be due to omitted physics in the model (for example, the absence of remote forcing farther upstream of the model domain). Nevertheless, the magnitude of the Goa current still remains stronger.

4.2. Experiment 2: Effect of Remote winds

We observe several events of poleward propagation with the amplitude of the current decreasing polewards (see for example, Figure 4a,b). In case of periods higher than 10 days, the local winds are weak and remote winds are strong (Figure 3c).

To capture the effect of remote winds, we force the model with a wind forcing decreasing poleward with latitude, i.e.

$$\tau = \frac{A}{N^2} \sin(\omega t), \quad (7)$$

where N is the block number, we observe propagation events with the current at the south leading the

current farther north (Figure 11). As expected, friction damps the poleward-propagating waves and reduces their amplitude.

It is to be noted that the drop in amplitude of current as the wave propagates poleward is sensitive to the friction coefficient used in the model. Even though the contribution of wind from the local blocks is small, the magnitude of current at Goa is not reduced significantly due to weak friction. For a very low friction coefficient, even a weak local forcing (such as Equation 7) can cause the magnitude of Goa currents to be comparable or even larger than Bhatkal currents.

4.3. Experiment 3: Propagating wind forcing

What happens when the wind forcing itself shows propagation? For instance, consider a case of travelling wind observed in Figure 8a,b from 15 to 25 June. The wind appears to travel poleward from Bhatkal to Goa and equatorward from Goa to Jaigarh.

To identify the response in currents, we assume the wind forcing of the form

$$\tau = A \sin l(ct \mp y), \quad (8)$$

where l is the wavenumber and c is the wind phase velocity. The wind's lag/lead between stations is determined by the phase velocity (c) (Figure 12, 13).

For a poleward-travelling wind, the current leads the wind and is strongest at Goa (Figure 12). As the wind phase speed approaches the first-mode CTW speed ($\sim 3.6 \text{ m s}^{-1}$), the wind and current are in phase. Also, the magnitude of the current decreases with c at all stations. The difference is not as evident from Figure 12f to Figure 12d, but the magnitude does show a slight decrease from 54 cm s^{-1} to 51 cm s^{-1} . We use the solution for barotropic shelf waves without friction from Gill & Schumann (1974) to explain this decrease in magnitude with c . The solution can be written as

$$\phi_n = \frac{2b_n A}{fl(1 - \frac{c}{c_n})} \sin \left[\frac{l}{2} \left(1 - \frac{c}{c_n} \right) y \right] \sin \left[\frac{l}{2} \left(1 + \frac{c}{c_n} \right) y - lct \right] \quad (9)$$

The first multiple in the RHS of Equation 9 shows that the magnitude of the current decreases with c , and the second multiple shows that the magnitude varies sinusoidally with distance. The resultant magnitude would be a combination of both these multiples. In our case, for both the periods, the magnitude of current drops with the wind phase speed. In the limit $c \rightarrow c_n$, we get,

$$\phi_n(y,t) = \frac{b_n A y}{f} \sin l(y - c_n t), \quad (10)$$

and the magnitude of the current, for constant f and b_n , increases with latitude.

For an equatorward-travelling wind forcing, it would appear as if the wave is propagating equatorward (Figure 13). Here, the current at the north leads the current farther south. As with poleward propagating wind, the amplitude of the currents weakens with wind phase velocity. It is to be noted that the wind leads the current on all occasions. The weak current at Jaigarh for both cases is due to change in shelf profile, which modifies the eigenfunction (F_n).

When QuikSCAT winds shows propagation, the expected response in currents is seen with the Bhatkal and Jaigarh station leading the Goa (see figure 8b,c from 13–23 June). Though the model simulation with QuikSCAT winds is able to pick this phase shift, the lead/lag is not as prominent as seen in observations (Figure 8d).

4.4. Experiment 4: Influence of higher-order modes

A distinct phase difference between sea level and current had been observed by Shetye & Vijith (2013) at the mouth of Mandovi-Zuari estuarine system. The difference in the phase ranged from a few hours to a day or two. We compared the sea level from the same tide-gauge (see Figure 1 for location) to the nearshore currents and observed a similar phase difference (the sea level was leading the currents)(Figure 17a). The phase difference is smaller when the current is equatorward. We attribute this difference in phase between sea level and current to the addition of higher-order modes.

When higher-order modes were added, other than changing the magnitude of the current, the model generates a nearshore (offshore) phase lag (lead) with the first mode (Figure 14a). The nearshore phase lag is caused due to the slow phase speeds of higher-order modes. Farther offshore (beyond the first node of the second mode), the second cross-shore mode flips sign (Figure 16), resulting in a lead (Figure 14b). With depth, complication arises due to the addition of vertical modes. The influence of mode crossing is seen while simulating the shelf-edge currents. The direction of the second mode changes before the 100 m contour only at Jaigarh (Figure 16a), which further weakens the current (Figure 8e,f).

In case of the pressure, and therefore sea level, the first mode is much stronger compared to the higher-order modes. The addition of modes does not result in an appreciable phase change in the pressure field (unlike with the currents), and the pressure tends to lead the current in presence of

remote forcing. For example, for a model run with constant wind forcing along the coast (see Figure 15b for the 10-day period), the pressure leads the current by about 15-18 hours.

The CTW model is also able to reproduce the phase difference seen in observations (Figure 17b), but the magnitude of sea level is smaller compared to the observation. During this time, the remote (local) forcing is strong (weak) (Section 3), which results in a lag owing to the addition of slow-propagating, higher-order modes. The difference in magnitude (and phase) between different modes for both current and sea level is shown in Figure 18.

If the wind forcing can extend far enough such that the remote wave is in opposite phase with the locally-generated wave, then the pressure can lag the currents. See for example the 4-day period wave in Figure 15. In this case, however, the lag was just a few hours. At such short time-scales, a lag can also be generated due to mass adjustment that follows the circulation.

5. Discussion

Evidence for propagation of CTWs have been shown from several parts of the world (see Mysak (1980) for a brief review). In most cases, the CTWs were identified by computing the coherence and phase difference between the adjusted sea level or any hydrodynamic variables at different location. The periodicity of the waves was then linked to atmospheric forcing by generally computing a spectrum. Along the central west coast of India, a similar coherence was observed in the alongshore currents by Amol et al. (2012), with the observed phase speed being slightly lower than the theoretical first-mode phase speed of CTWs (Amol, 2014). The coherence was more evident on the shelf currents compared to the slope currents. Amol et al. (2012) used a linear shelf model to identify the role of CTWs on generating such phase changes.

Though evidence for CTWs were noted over the shelf along the central west coast of India, earlier observations showed a distinct difference between the nearshore and shelf-edge currents. The CTWs being more evident near the shelf edge than near shore. The absence of remote waves near the shore was shown by Shetye et al. (2008), who noticed a strong lag correlation between local winds and the nearshore currents (with the wind leading the current). This, in turn, led them to conclude that the high-frequency currents were primarily driven by local winds, and the remote waves were probably damped owing to strong friction. As the depth of water column increases, the role of friction weakens, leading to the presence of CTWs near the shelf edge. Carrying out a similar analysis with a more recent set of current meters, we have identified that, even at periods shorter than 10 days, the influence of remote forcing on nearshore currents is quite evident. Which implies that the measurements shown by Shetye et al. (2008) were probably made when the local (remote) forcing

was strong (weak), and this in turn resulted in a good correlation between the winds and currents with the winds leading the currents. Further, calculations from CTW model show that even a good lag correlation between local wind and local current does not necessarily imply absence of remote forcing (see Figure 3d and experiments from Section 4). With the right kind of wind forcing, the remotely generated waves can cause an increase or decrease in lag/lead between local currents and wind. Therefore, the wind-current phase difference observed by Shetye et al. (2008) could also have been caused by combination of local and remote winds rather than just the local winds.

The CTW model with restricted model domain is able to capture the currents reasonably well, which suggests that unlike the seasonal cycle of WICC, the high-frequency WICC is primarily driven by west coast winds. Earlier modelling studies (McCreary et al., 1993; Shankar et al., 2002; Suresh et al., 2013) have suggested that in order to simulate currents along the west coast of India, in particular at seasonal and intraseasonal time scales, one has to take the entire North Indian Ocean basin into consideration. The small size of the basin, bounded by land mass in the north and the region being in proximity to the equator, allows the large-scale planetary and coastal waves to carry information faster across the basin. Winds along east coast of India and even equator are known to have considerable effect on WICC. Our results show that models with domains restricted to the west coast of India would still be able to capture shelf WICC, but only in frequency bands ranging from a few days to a few weeks, which is sometimes referred as the ‘weather band’. In addition, as shown in Figure 6 or by Amol et al. (2012), the winds in Gulf of Mannar, off the coast of Sri Lanka and east coast of India cannot be neglected. The wind in Gulf of Mannar (the region between India and Sri Lanka) is of particular interest since its effect would be felt primarily on the shelf circulation and not on the slope. The coastline in this region also meanders in a complex manner, and Wilkin & Chapman (1987) have suggested that such strong discontinuities along the coast would scatter free shelf waves into all permissible modes. A similar effect would also be seen in the northwest coast of India, where the coastline sharply changes at $\sim 21^\circ$ N. Other changes in bathymetry profile, like the widening of shelf width, could also have profound effect on the shelf WICC. For instance, the amplitude of current, as shown by solutions of Gill & Schumann (1974), is seen to increase poleward till Goa, but the widening of shelf north of Goa weakens the poleward propagating CTWs. In short it is the combination of bathymetry and remote forcing that causes the current at Goa to be stronger compared to its contemporary stations in the north and south. It is to be noted that the first-mode CTW phase speed increases from south to north (Table 2). The calculated phase speed at Jaigarh is almost thrice as fast as that obtained along the southern tip of India, which implies that the currents at north would respond more quickly to the remote forcing compared to the south.

Observation from ADCPs also reflect the effect of travelling winds on currents on an isolated occasion. The currents between two stations is seen to lead or lag each other in parallel with the wind. Gill & Schumann (1974) had shown that such propagating solutions can be obtained when the wind effects are ignored beyond a certain point. They also showed that if we include the wind stress acting at some initial time, the response is generated in two different frequencies: one that propagates with the forcing system and the other in the direction of free shelf waves. Further, the wind may lead or lag the current depending on the direction in which the wind travels, and strength of remote winds.

A similar difference in phase between the sea level and currents is seen off the central west coast of India and could be attributed to the addition of remotely-forced higher-order-mode CTWs. Unlike for the sea level, the magnitude of the second and third modes in currents is comparable to the first mode. These slowly-propagating remotely-forced higher-order modes tend to generate a lead/lag in currents but not the sea level. The caveat here is that we have neglected the influence of modes higher than 3. Clarke & Van Gorder (1986) have shown that it would require more than 7 modes to simulate the alongshore currents accurately. Earlier studies on CTWs have shown reasonable success in hindcasting currents with a single mode (Brink, 1982a; Battisti & Hickey, 1984; Amol et al., 2012). The dominance of a particular mode, however, would vary from region to region. For example, Church et al. (1986) noted that over a certain section along the East Australian shelf, the mode 2 carried a greater fraction of CTW energy compared to mode 1. Model results that are dependent on higher-order modes (> 3) are generally a suspect because the friction and wind-coupling coefficients for these modes are highly sensitive to small changes in stratification and bathymetry profile. Along the west coast of India, the CTW model with first mode is able to capture the observed variability reasonably well (see Section 3). Nevertheless, the influence of higher-order modes cannot be neglected especially in determining lead/lag between currents and sea level (or currents and winds).

In spite of all the model limitations, the shelf WICC tends to show modulations that corresponds to propagation of long coastal-trapped waves. Many of the observed features, such as strong currents at Goa or the observed phase lag between sea level and currents, could be explained using simple linear wave dynamics. Our results hinge on the fact that the model is highly responsive to changes in wind stress but relatively insensitive to reasonable changes in other model inputs (see sensitivity analysis of the model by Chapman (1987) along the California coast). Yet, there are several occasions where the model fails to capture the observed variability. This difference could be either attributed to the omitted dynamics in the model or to an error in the model inputs. For example, the physical processes that cannot be incorporated in the model, like the cross-shore variations in the wind field

or stratification, could affect the dynamics between the nearshore and shelf-edge circulation. Also, the linear model does not account for temporal variations in the density profile due to freshwater discharges from west-coast rivers or the low-saline (high-saline) water flux from the southwestern Bay of Bengal (northern Arabian Sea). These processes would be important to understand the heterogeneous nature of the WICC. Comparison with the currents simulated by a full-fledged general circulation model would help resolve several of these issues (such as the effect of sharp changes in coastlines at Gulf of Mannar) and could be a subject of future paper.

The significant role of remote forcing for currents on the shelf, especially the inner shelf, has serious implications for environmental impact assessments (EIAs). The EIA measurements are typically carried out near the shore and our analysis suggests that the propagation of CTWs will have an impact on near-coastal currents at locations remote from the forcing region. Also, if the inference that the forcing for the west-coast shelf extends into the Gulf of Mannar or the east coast of Sri Lanka applies to the inner shelf as well, then EIA models will have to include this remote-forcing effect. Moreover, a recent study suggests that the influence of CTWs may even extend to estuarine systems located along the west coast of India (Shetye & Vijith, 2013). The disturbance generated by these waves is seen to propagate undamped as far as ~40 km into an estuarine channel.

6. Acknowledgement

We would like to thank Dr. Shankar and Prof. Vinayachandran for their comments on the application of CTW theory. We would also like to acknowledge Dr. Sanil Kumar and colleagues from Oceanographic Mooring Group of CSIR-NIO - namely Yogesh, Khalap, Narayan, Mithun and Prakash Tari - in various cruises of Sagar Manjusha and Sindhu Sankhalp for collection of long-term in-situ current data. The CTW codes are obtained from <http://www.whoi.edu/filesserver.do?id=60003&pt=2&p=35366>. The QuikSCAT data was downloaded from <http://www.ifremer.fr/cersat/en/data/download/download.htm>. All figures were created using Generic Mapping Tools (GMT) and Ferret. Funding for this work was provided by Council of Scientific & Industrial Research (CSIR) through Supra-Institutional Project during 2007–2012 and Ocean Finder from 2012 onwards, by ESSO-INCOIS under the Ocean Observing Systems programme of the Ministry of Earth Sciences, New Delhi, and by Science and Engineering Research Board, Department of Science and Technology. A part of this work is from the doctoral research, carried out at CSIR-National Institute of Oceanography, by P. Amol. This is CSIR-NIO contribution no. XXXX.

References

- Amol, P. (2014). *Intraseasonal variability of currents along west coast of India*. Ph.D. thesis Goa University.
- Amol, P., Shankar, D., Aparna, S. G., Shenoi, S. S. C., Fernando, V., Shetye, S. R., Mukherjee, A., Agarvadekar, Y., Khalap, S., & Satelkar, N. P. (2012). Observational evidence from direct current measurements for propagation of remotely forced waves on the shelf off the west coast of India. *Journal of Geophysical Research: Oceans*, *117*, n/a–n/a. doi:[10.1029/2011JC007606](https://doi.org/10.1029/2011JC007606). C05017.
- Amol, P., Shankar, D., Fernando, V., Mukherjee, A., Aparna, S., Fernandes, R., Michael, G., Khalap, S., Satelkar, N., Agarvadekar, Y., Gaonkar, M., Tari, A., Kankonkar, A., & Vernekar, S. (2014). Observed intraseasonal and seasonal variability of the West India Coastal Current on the continental slope. *Journal of Earth System Science*, *123*, 1045–1074. doi:[10.1007/s12040-014-0449-5](https://doi.org/10.1007/s12040-014-0449-5).
- Aparna, M., Shetye, S. R., Shankar, D., Shenoi, S. S. C., Mehra, P., & Desai, R. G. P. (2005). Estimating the seaward extent of sea breeze from quikscat scatterometry. *Geophysical Research Letters*, *32*, n/a–n/a. doi:[10.1029/2005GL023107](https://doi.org/10.1029/2005GL023107). L13601.
- Battisti, D. S., & Hickey, B. M. (1984). Application of remote wind-forced coastal trapped wave theory to the oregon and washington coasts. *Journal of Physical Oceanography*, *14*, 887–903. doi:[10.1175/1520-0485\(1984\)014<0887:AORWFC>2.0.CO;2](https://doi.org/10.1175/1520-0485(1984)014<0887:AORWFC>2.0.CO;2).
- Bell, C., Vassie, J. M., & L., W. P. (1998). *POL/PSMSL Tidal Analysis Software Kit 2000 (TASK-2000)*. Technical Report Permanent Service for Mean Sea Level, Proudman Oceanographic Laboratory.
- Brink, K. H. (1982a). A comparison of long coastal trapped wave theory with observations off Peru. *Journal of Physical Oceanography*, *12*, 897–913. doi:[10.1175/1520-0485\(1982\)012<0897:ACOLCT>2.0.CO;2](https://doi.org/10.1175/1520-0485(1982)012<0897:ACOLCT>2.0.CO;2).
- Brink, K. H. (1982b). The effect of bottom friction on low-frequency coastal trapped waves. *Journal of Physical Oceanography*, *12*, 127–133. doi:[10.1175/1520-0485\(1982\)012<0127:TEOBFO>2.0.CO;2](https://doi.org/10.1175/1520-0485(1982)012<0127:TEOBFO>2.0.CO;2).
- Brink, K. H., & Chapman, D. C. (1987). *Programs for computing properties of coastal-trapped waves and wind-driven motions over the continental shelf and slope*. Technical Report Woods Hole Oceanographic Institution. Second Edition.
- Chapman, D. C. (1987). Application of wind-forced, long, coastal-trapped wave theory along the california coast. *Journal of Geophysical Research: Oceans*, *92*, 1798–1816. doi:[10.1029/JC092iC02p01798](https://doi.org/10.1029/JC092iC02p01798).
- Chatterjee, A., Shankar, D., Shenoi, S. S. C., Reddy, G. V., Michael, G. S., Ravichandran, M., Gopalkrishna, V. V., Rao, E. P. R., Bhaskar, T. V. S. U., & Sanjeevan, V. N. (2012). A new atlas of temperature and salinity for the North Indian Ocean. *Journal of Earth System Science*, *121*, 559–593.
- Church, J. A., White, N. J., Clarke, A. J., Freeland, H. J., & Smith, R. L. (1986). Coastal-trapped waves on the east australian continental shelf part ii: Model verification. *Journal of Physical Oceanography*, *16*, 1945–1957. doi:[10.1175/1520-0485\(1986\)016<1945:CTWOTE>2.0.CO;2](https://doi.org/10.1175/1520-0485(1986)016<1945:CTWOTE>2.0.CO;2).
- Clarke, A. J., & Van Gorder, S. (1986). A method for estimating wind-driven frictional, time-

dependent, stratified shelf and slope water flow. *Journal of Physical Oceanography*, *16*, 1013–1028. doi:[10.1175/1520-0485\(1986\)016<1013:AMFEWD>2.0.CO;2](https://doi.org/10.1175/1520-0485(1986)016<1013:AMFEWD>2.0.CO;2).

Dee, D. P., Uppala, S. M., Simmons, A. J., Berrisford, P., Poli, P., Kobayashi, S., Andrae, U., Balmaseda, M. A., Balsamo, G., Bauer, P., Bechtold, P., Beljaars, A. C. M., van de Berg, L., Bidlot, J., Bormann, N., Delsol, C., Dragani, R., Fuentes, M., Geer, A. J., Haimberger, L., Healy, S. B., Hersbach, H., Hlm, E. V., Isaksen, L., Kllberg, P., Khler, M., Matricardi, M., McNally, A. P., Monge-Sanz, B. M., Morcrette, J.-J., Park, B.-K., Peubey, C., de Rosnay, P., Tavolato, C., Thpaut, J.-N., & Vitart, F. (2011). The era-interim reanalysis: configuration and performance of the data assimilation system. *Quarterly Journal of the Royal Meteorological Society*, *137*, 553–597. doi:[10.1002/qj.828](https://doi.org/10.1002/qj.828).

Gill, A. E., & Schumann, E. H. (1974). The generation of long shelf waves by the wind. *Journal of Physical Oceanography*, *4*, 83–90. doi:[10.1175/1520-0485\(1974\)004<0083:TGOLSW>2.0.CO;2](https://doi.org/10.1175/1520-0485(1974)004<0083:TGOLSW>2.0.CO;2).

Johnson, E. S., Bonjean, F., Lagerloef, G. S. E., Gunn, J. T., & Mitchum, G. T. (2007). Validation and error analysis of oscar sea surface currents. *Journal of Atmospheric and Oceanic Technology*, *24*, 688–701. doi:[10.1175/JTECH1971.1](https://doi.org/10.1175/JTECH1971.1).

McCreary, J. P., Kundu, P. K., & Molinari, R. L. (1993). A numerical investigation of dynamics, thermodynamics and mixed-layer processes in the Indian Ocean. *Progress in Oceanography*, *31*, 181–244. doi:[10.1016/0079-6611\(93\)90002-U](https://doi.org/10.1016/0079-6611(93)90002-U).

Mukherjee, A., Shankar, D., Fernando, V., Amol, P., Aparna, S., Fernandes, R., Michael, G., Khalap, S., Satelkar, N., Agarvadekar, Y., Gaonkar, M., Tari, A., Kankonkar, A., & Vernekar, S. (2014). Observed seasonal and intraseasonal variability of the East India Coastal Current on the continental slope. *Journal of Earth System Science*, *123*, 1197–1232. doi:[10.1007/s12040-014-0471-7](https://doi.org/10.1007/s12040-014-0471-7).

Mysak, L. A. (1980). Recent advances in shelf wave dynamics. *Reviews of Geophysics*, *18*, 211–241. doi:[10.1029/RG018i001p00211](https://doi.org/10.1029/RG018i001p00211).

Shankar, D., & Shetye, S. R. (1997). On the dynamics of the Lakshadweep high and low in the southeastern Arabian Sea. *Journal of Geophysical Research: Oceans*, *102*, 12551–12562. doi:[10.1029/97JC00465](https://doi.org/10.1029/97JC00465).

Shankar, D., Vinayachandran, P., & Unnikrishnan, A. (2002). The monsoon currents in the north Indian Ocean. *Progress in Oceanography*, *52*, 63–120. doi:[http://dx.doi.org/10.1016/S0079-6611\(02\)00024-1](http://dx.doi.org/10.1016/S0079-6611(02)00024-1).

Shetye, S., & Vijith, V. (2013). Sub-tidal water-level oscillations in the Mandovi estuary, west coast of India. *Estuarine, Coastal and Shelf Science*, *134*, 1–10. doi:[10.1016/j.ecss.2013.09.016](https://doi.org/10.1016/j.ecss.2013.09.016).

Shetye, S. R., Suresh, I., Shankar, D., Sundar, D., Jayakumar, S., Mehra, P., Prabhudesai, R. G., & Pednekar, P. S. (2008). Observational evidence for remote forcing of the West India Coastal Current. *Journal of Geophysical Research: Oceans*, *113*, n/a–n/a. doi:[10.1029/2008JC004874](https://doi.org/10.1029/2008JC004874). C11001.

Sindhu, B., Suresh, I., Unnikrishnan, A., Bhatkar, N., Neetu, S., & Michael, G. (2007). Improved bathymetric datasets for the shallow water regions in the Indian Ocean. *Journal of Earth System Science*, *116*, 261–274. doi:[10.1007/s12040-007-0025-3](https://doi.org/10.1007/s12040-007-0025-3).

Suresh, I., Vialard, J., Lengaigne, M., Han, W., McCreary, J., Durand, F., & Muraleedharan, P. M. (2013). Origins of wind-driven intraseasonal sea level variations in the north indian ocean coastal waveguide. *Geophysical Research Letters*, *40*, 5740–5744.

Wilkin, J. L., & Chapman, D. C. (1987). Scattering of continental shelf waves at a discontinuity in shelf width. *Journal of Physical Oceanography*, *17*, 713–724. doi:[10.1175/1520-0485\(1987\)017<0713:SOCSWA>2.0.CO;2](https://doi.org/10.1175/1520-0485(1987)017<0713:SOCSWA>2.0.CO;2).

No.	Instrument	Station	Latitude	Longitude	Measurement	Water	Sampling	Angle	Start	End
			$^{\circ}$ N	$^{\circ}$ E	depth (m)	Depth	Interval (min)	(deg)	Date	Date
C1	Current meter	Bhatkal	13.31 $^{\circ}$ N	74.62 $^{\circ}$ E	4	20	10	19	13 Mar 2008	13 Apr 2008
C2	Current meter	Goa	15.54 $^{\circ}$ N	73.61 $^{\circ}$ E	5	35	10	28	09 Mar 2008	15 Apr 2008
C3	Current meter	Jaigarh	17.06 $^{\circ}$ N	73.13 $^{\circ}$ E	5	30	10	16	27 Feb 2008	11 Apr 2008
A1	ADCP (1 year)	Goa	15.15 $^{\circ}$ N	73.05 $^{\circ}$ E	16–160	173	30	14	29 Oct 2011	02 Oct 2012
A2	ADCP	Bhatkal	13.67 $^{\circ}$ N	73.51 $^{\circ}$ E	12–96	104	15	-1	05 Mar 2008	07 Sep 2008
A3	ADCP	Goa	15.17 $^{\circ}$ N	73.19 $^{\circ}$ E	12–88	98	15	14	02 Mar 2008	22 Oct 2008
A4	ADCP	Jaigarh	17.15 $^{\circ}$ N	72.08 $^{\circ}$ E	12–92	108	15	20	04 Mar 2008	18 Oct 2008
T1	Tide gauge	Goa	15.50 $^{\circ}$ N	73.81 $^{\circ}$ E	4.5	4.5	5	-	01 Mar 2008	30 Apr 2008
W1	Anemometer	Goa	15.46 $^{\circ}$ N	73.80 $^{\circ}$ E	48	-	10	27	01 Mar 2008	30 Apr 2008

Table 1: The ADCPs are upward looking and has a bin size of 4 m. The measurement range is given in column 6. All ADCPs except A1 are 75 kHz, and extends for a period of ~7 months. The one-year ADCP (A1) is 150 kHz and is deployed at a deeper water-column depth (see column 7). The angle of rotation for determining the alongshore component is provided in column 9. The angle is obtained by minimizing the cross-shore component (coast angle) for currents (winds), and is calculated anti-clockwise from north. The height above mean sea level for anemometer is provided in column 6. Note that all measurements except A1 are during 2008. The data from A1 ADCP was collected during 2011–2012.

Latitude (° N)	c_1 (m s ⁻¹)	b_1 (cm ^{-1/2} s ⁻¹)	a_{11} (cm) X 10 ⁻⁹
08.5	2.3360	2.2468	5.7250
09.5	2.3770	2.1456	5.5686
10.5	2.4243	2.1665	6.2922
11.5	2.9274	2.4045	7.6477
12.5	2.8496	2.1084	6.3895
13.5	3.8753	2.4540	7.6085
14.5	3.8283	2.2866	6.9756
15.5	3.5496	2.1610	7.0773
16.5	4.4138	1.8628	4.7854
17.5	6.7000	2.0656	4.1676

Table 2: CTW model parameters shown at different latitudes.

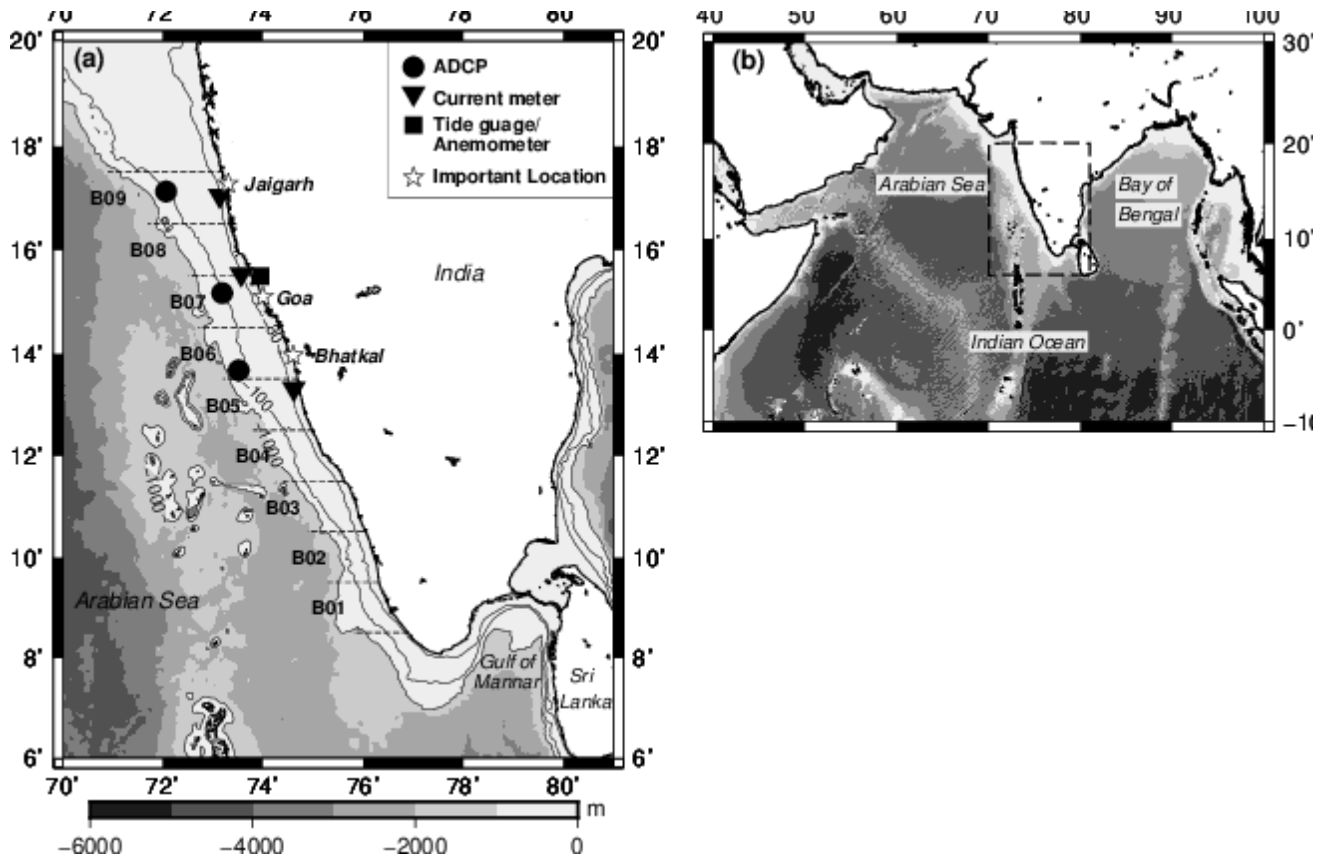


Figure 1: (a) Map of west coast of India showing mooring locations. The ADCP (current meter) moorings were deployed on the shelf at 100 m (30 m) water-column depth. The anemometer was located on the rooftop of CSIR-National Institute of Oceanography, Goa. The tide-gauge was located near the mouth of the Mandovi estuary, Goa. The dashed lines, which represents the model grid, divide the west coast into nine blocks of 1° each (B1–B9). The model domain extends from 8.5° N (B1) to 17.5° N (B9). (b) Map showing location of region of interest in the North Indian Ocean. The bathymetry is from (Sindhu et al., 2007).

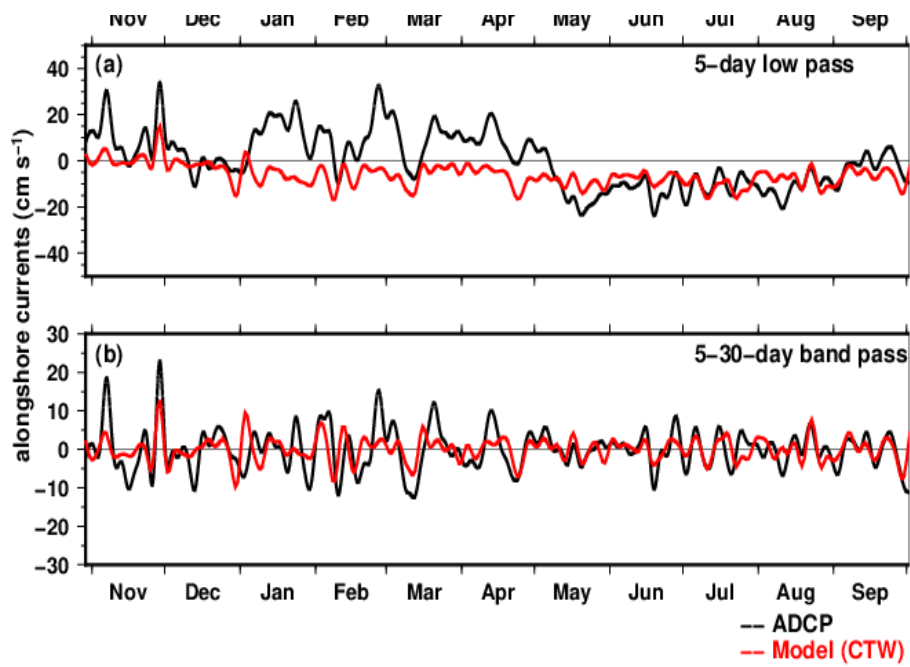


Figure 2: (a) Comparison between observed 5-day low-pass shelf-edge current (black) and modelled (CTW theory) current (red) at Goa. (b) Similar comparison, but for 5–30-day band-passed current. The currents are shown at 16 m depth.

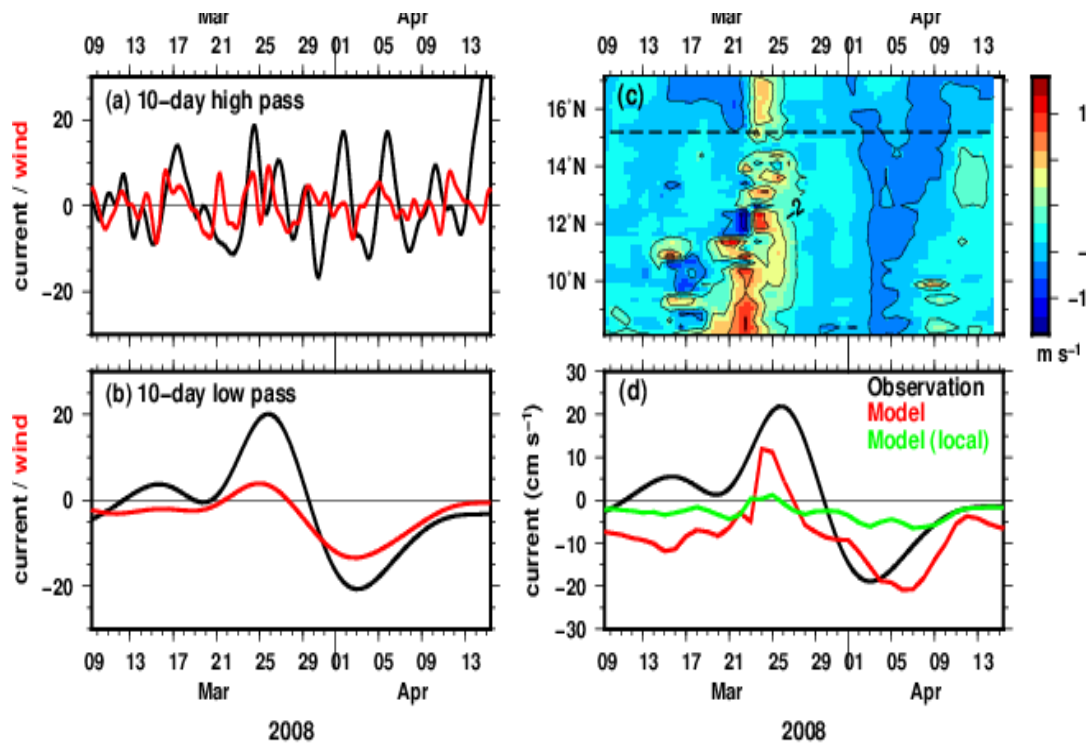


Figure 3: (a) 10 day high-pass nearshore current (cm s^{-1}) and wind (dm s^{-1}) at Goa. The wind data is from automated weather station. (b) 10-day low-pass current and winds. (c) QuikSCAT winds (m s^{-1}) as a function of latitude and time. The dashed horizontal line shows the Goa mooring location. (d) Comparison of 10-day low-pass current (black) and modelled current (red). The contribution from the local block (B07 in Figure 1), or the locally forced current, is also shown (green). The remote contribution is the difference between the modelled and local currents. Note that a 1.3-day low-pass filter is applied to the high-pass currents to remove the diurnal cycle. The currents shown are at 5 m depth.

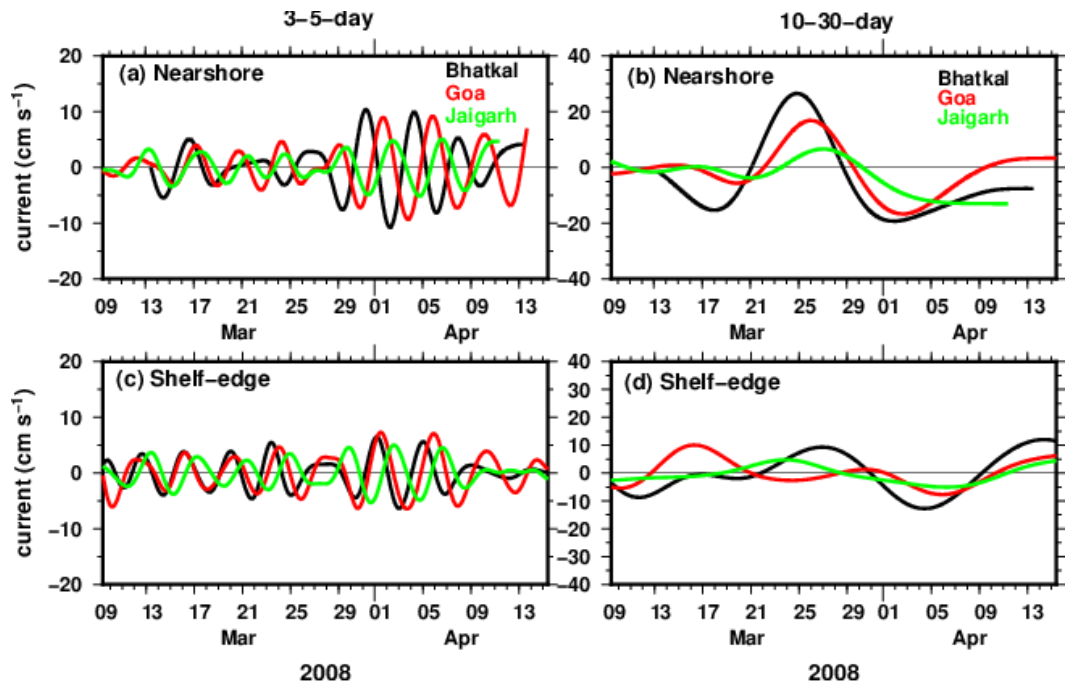


Figure 4: Nearshore currents at 5 m from current meters at Bhatkal (black), Goa (red), and Jaigarh (green) after applying a (a) 3-5-day and (b) 10-30-day band-pass filter. Shelf-edge currents at 12 m from ADCPs at same locations with (c) 3-5-day and (d) 10-30-day band-pass filter applied.

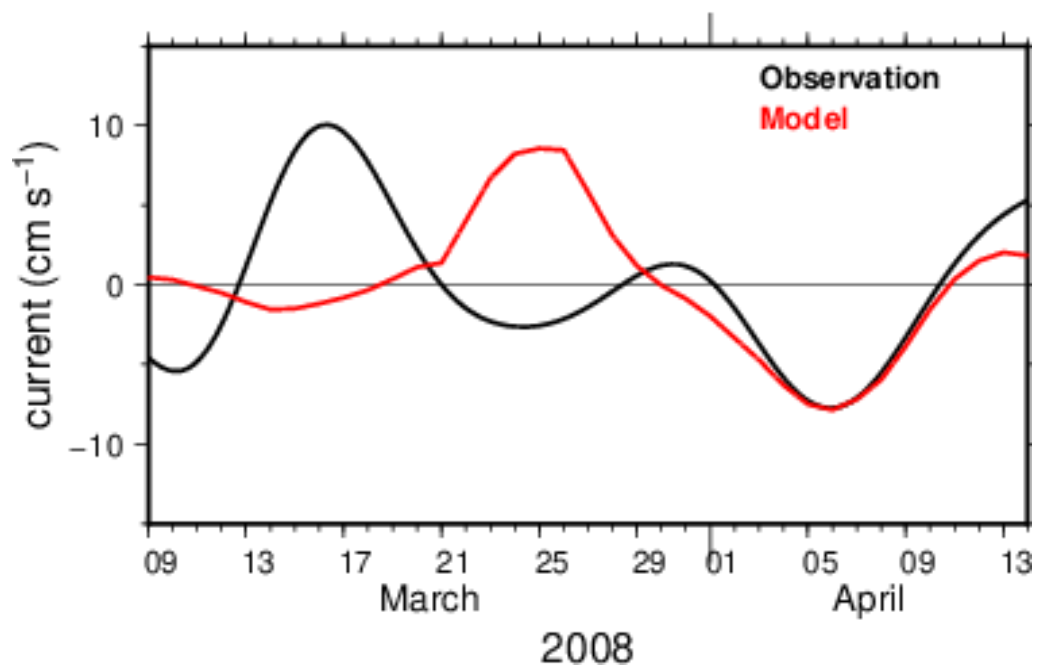


Figure 5: Comparison between 10–30-day band-pass shelf-edge currents from ADCP (black) and CTW model (red) at Goa. The currents are shown at 12 m depth.

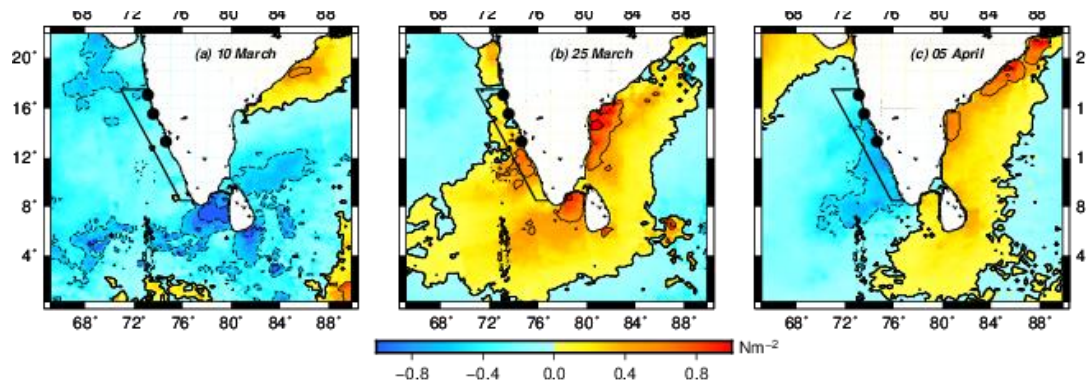


Figure 6: QuikSCAT meridional wind-stress on (a) 10 March 2008, (b) 25 March 2008, and (c) 05 April 2008. The black circles show the mooring location, and the slant box shows the model domain. The effect of strong winds south (and farther upstream) of the model domain is ignored in CTW calculations.

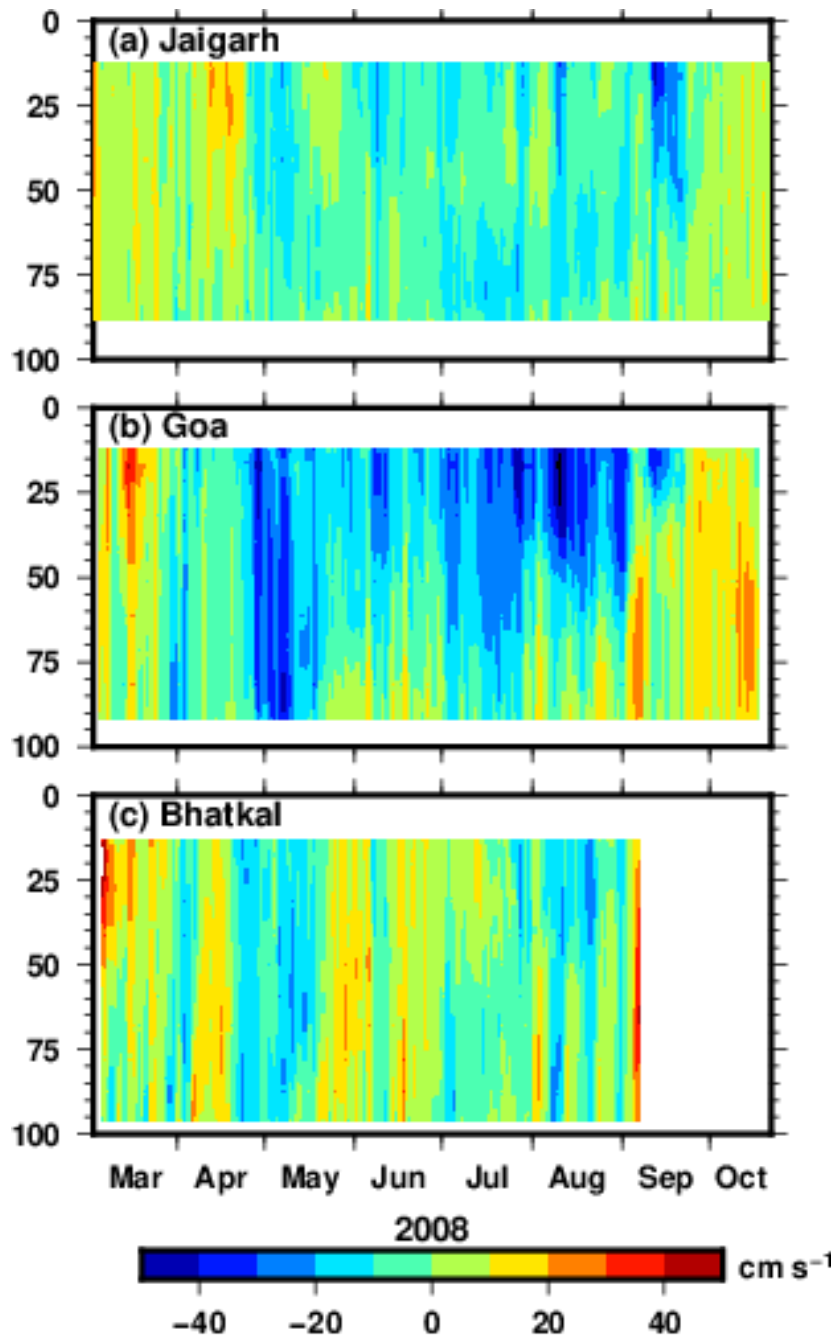


Figure 7: 2.5-day low-passed alongshore currents near the shelf-edge at (a) Jaigarh (17°), (b) Goa (15°), and (c) Bhatkal (13.5°). Strong currents are seen at Goa compared to Bhatkal and Jaigarh. Figure redrawn based on the data presented in Figure 2 of [Amol et al. \(2012\)](#).

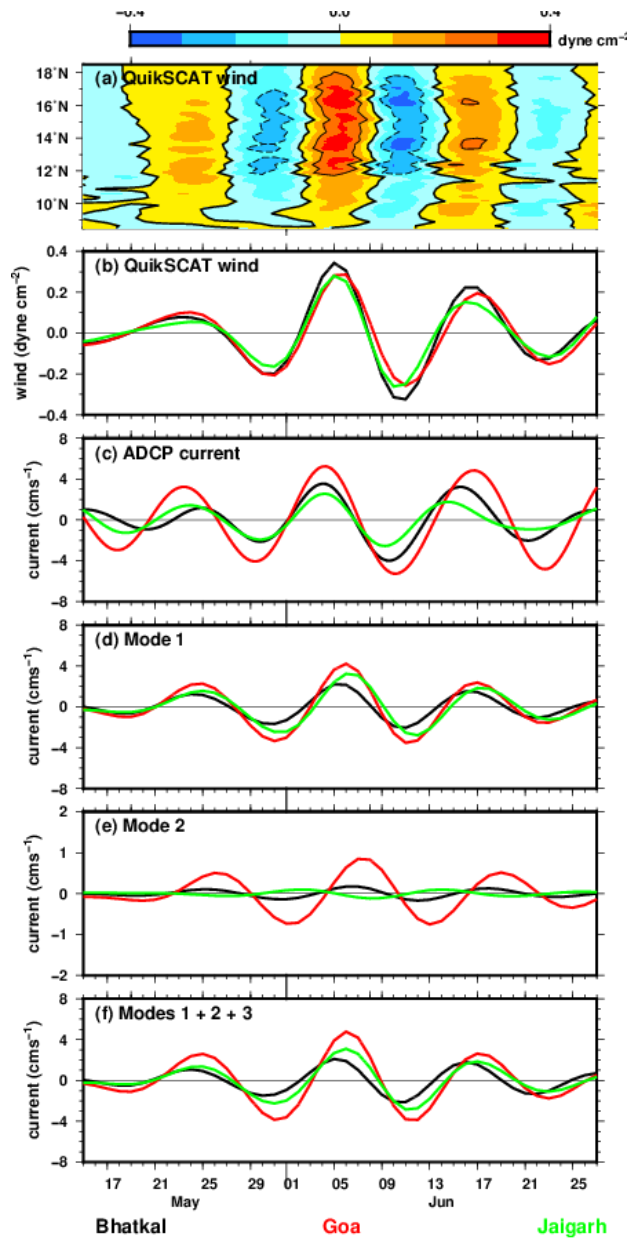


Figure 8: 10–14-day band-pass wind and current. (a) QuikSCAT wind stress as a function of latitude. (b) QuikSCAT wind stress shown for Bhatkal (black), Goa (Red), and Jaigarh (green). (c) Shelf-edge alongshore currents from ADCP. Currents from CTW model for (d) first mode, (e) second mode, and (f) summation of first three modes. The model is forced with QuikSCAT winds. Figure (a) and (c) redrawn based on the data presented in Figure 7 of [Amol et al. \(2012\)](#). The current data is shown at 12 m depth.

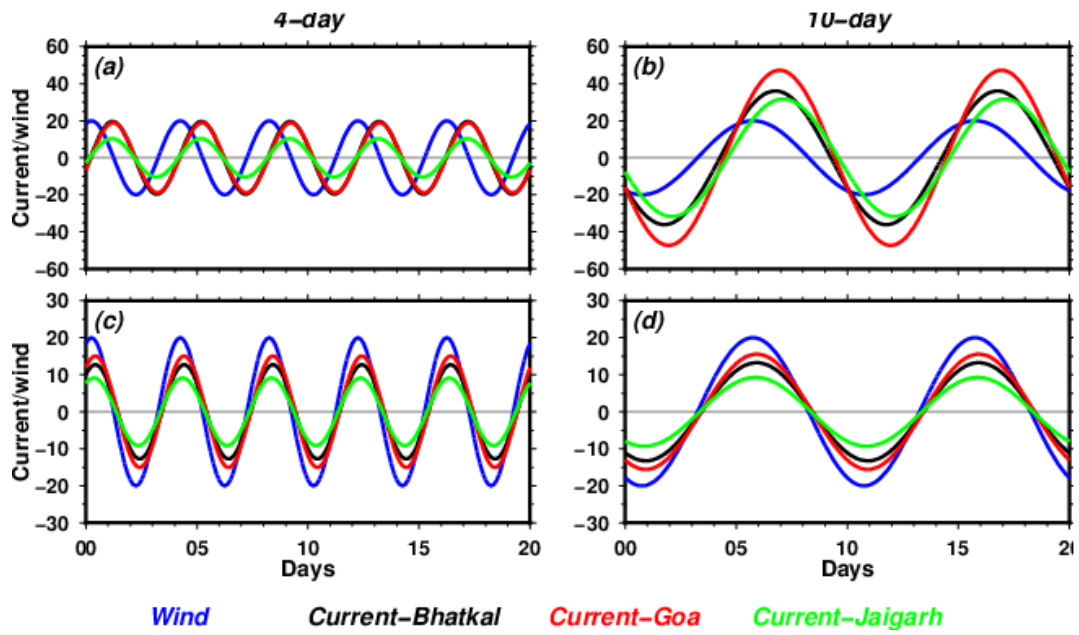


Figure 9: Results from Experiment 1. The model is forced with stationary winds with constant amplitude along the coast. The figure shows currents from CTW model and winds at Goa for (a) 4-day period and (b) 10-day period. The contribution of winds from the local block to the currents for the above periods are shown in panels (c) and (d), respectively. The sum of local and remote blocks gives the total current.

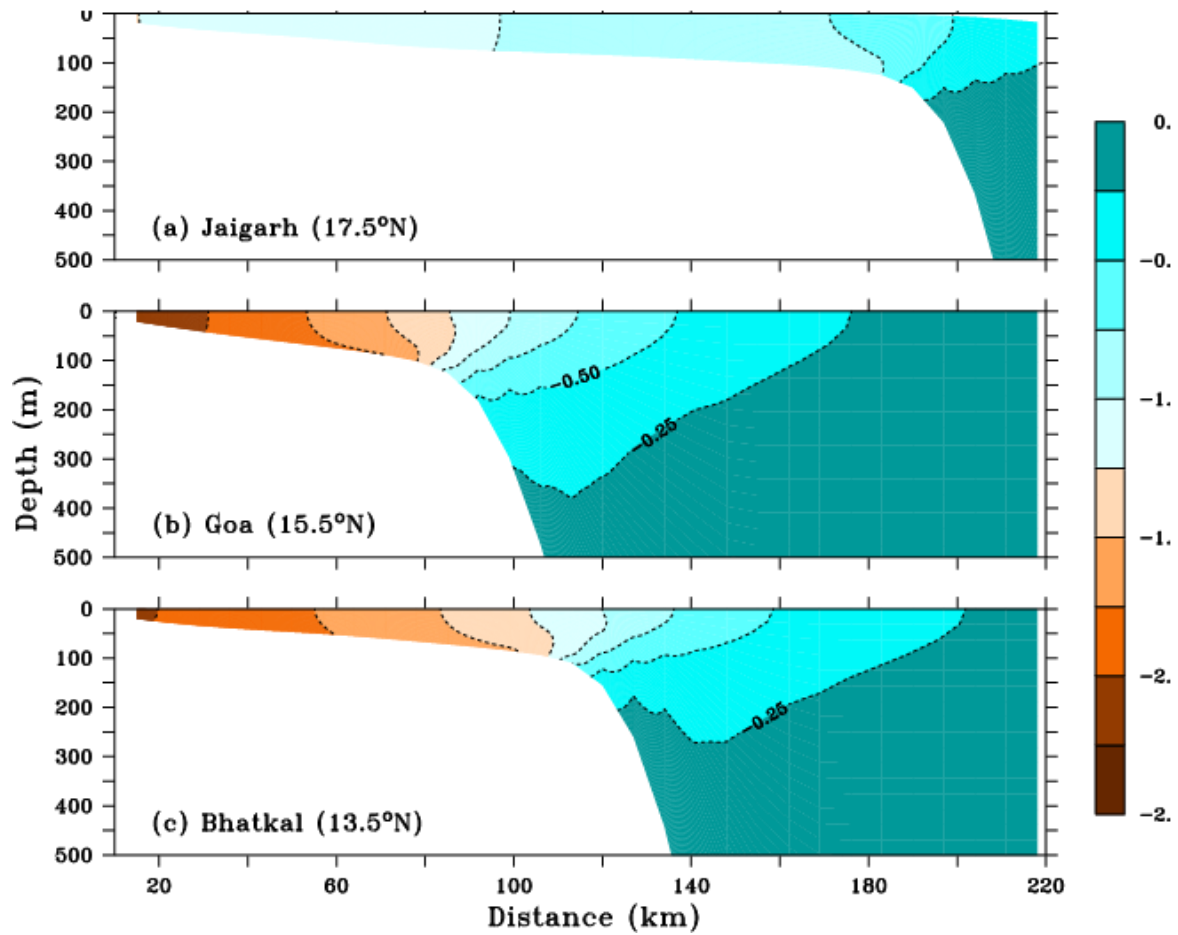


Figure 10: Offshore vertical structure for the first mode alongshore currents at (a) Jaigarh, (b) Goa, and (c) Bhatkal. The units are arbitrary, and only the top 500 m is shown.

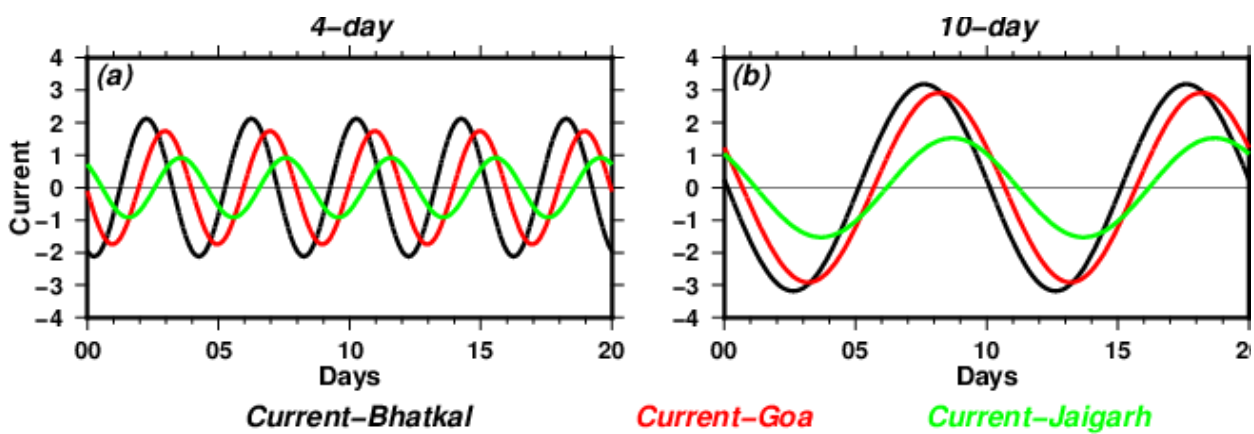


Figure 11: Results from Experiment 2. The model is forced with strong remote winds whose amplitude decreases poleward along the coast. Figure shows currents from CTW model for (a) 4-day period and (b) 10-day period.

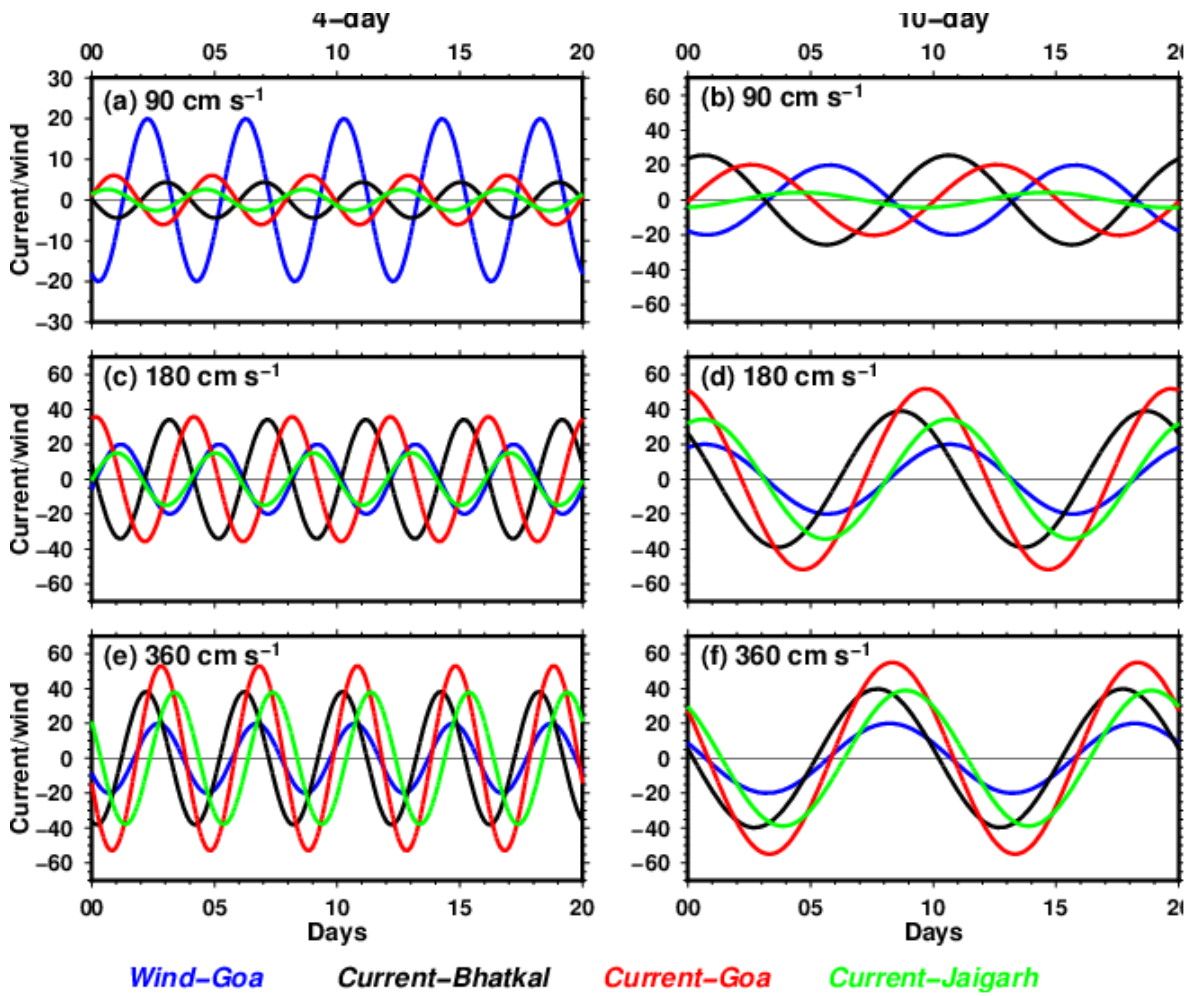


Figure 12: Results from Experiment 3. The model is forced with poleward propagating wind. Figure shows currents from CTW model and winds from Goa. The panel on the left (right) is for a 4-day (10-day) period. The wind phase speed is shown in the upper-left corner of the figures. The first-mode speed for the coastal-trapped wave is $\sim 3.6 \text{ m s}^{-1}$.

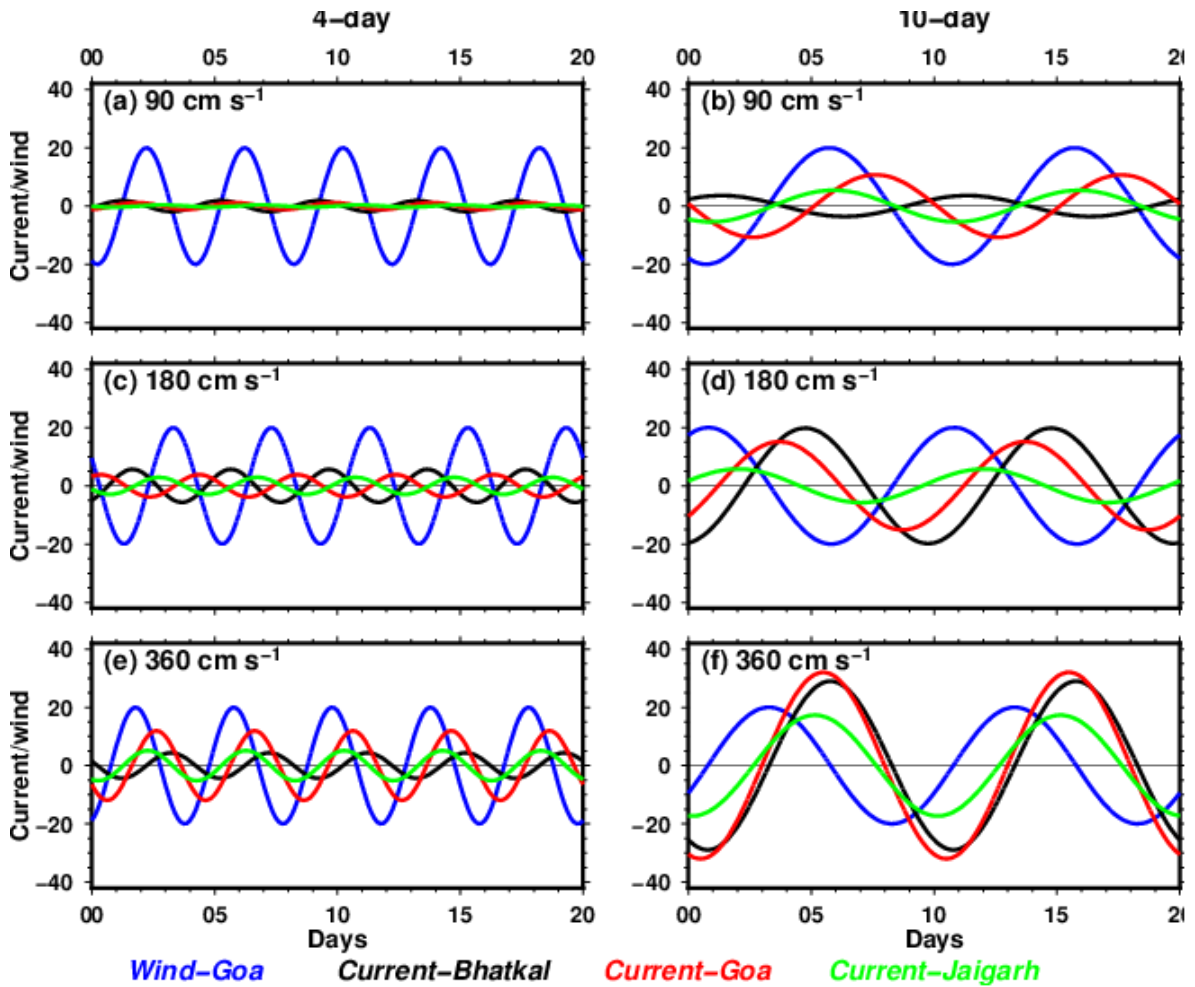


Figure 13: Results from Experiment 3. The model is forced with equatorward propagating winds. Figure shows currents from CTW model and winds from Goa. The panel on the left (right) is for a 4-day (10-day) period. The wind phase speed is shown in the upper-left corner of the figures. The first-mode speed for the coastally-trapped wave is $\sim 3.6 \text{ m s}^{-1}$.

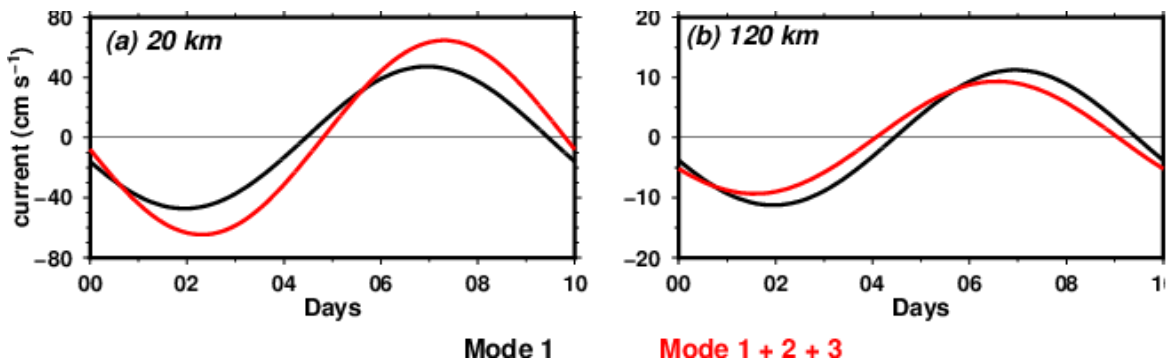


Figure 14: Results from Experiment 4. This experiment highlights the influence of higher-order modes for the nearshore and shelf-edge currents. The model was forced with stationary winds with constant amplitude along the coast. Currents from the CTW model for the first mode (black) and summation of first three modes (red) at a distance of (a) 20 km from the coast and (b) 120 km from the coast.

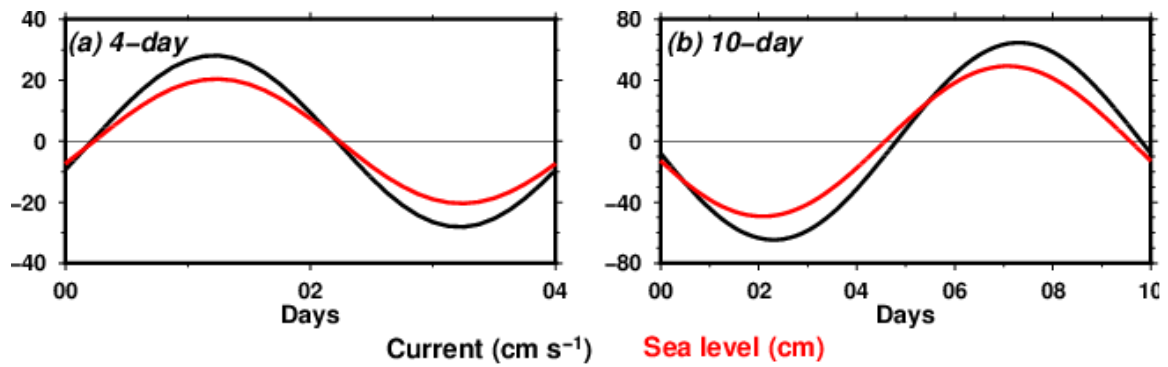


Figure 15: Results from Experiment 4. This experiment highlights the influence of higher-order modes on pressure and current. Figure shows current (black) and pressure (red) from the CTW model for (a) 4-day period and (b) 10-day period. The first three modes are summed for both current and pressure. The model was forced with stationary winds with constant amplitude along the coast. Note the difference in phase between pressure and current at different periods.

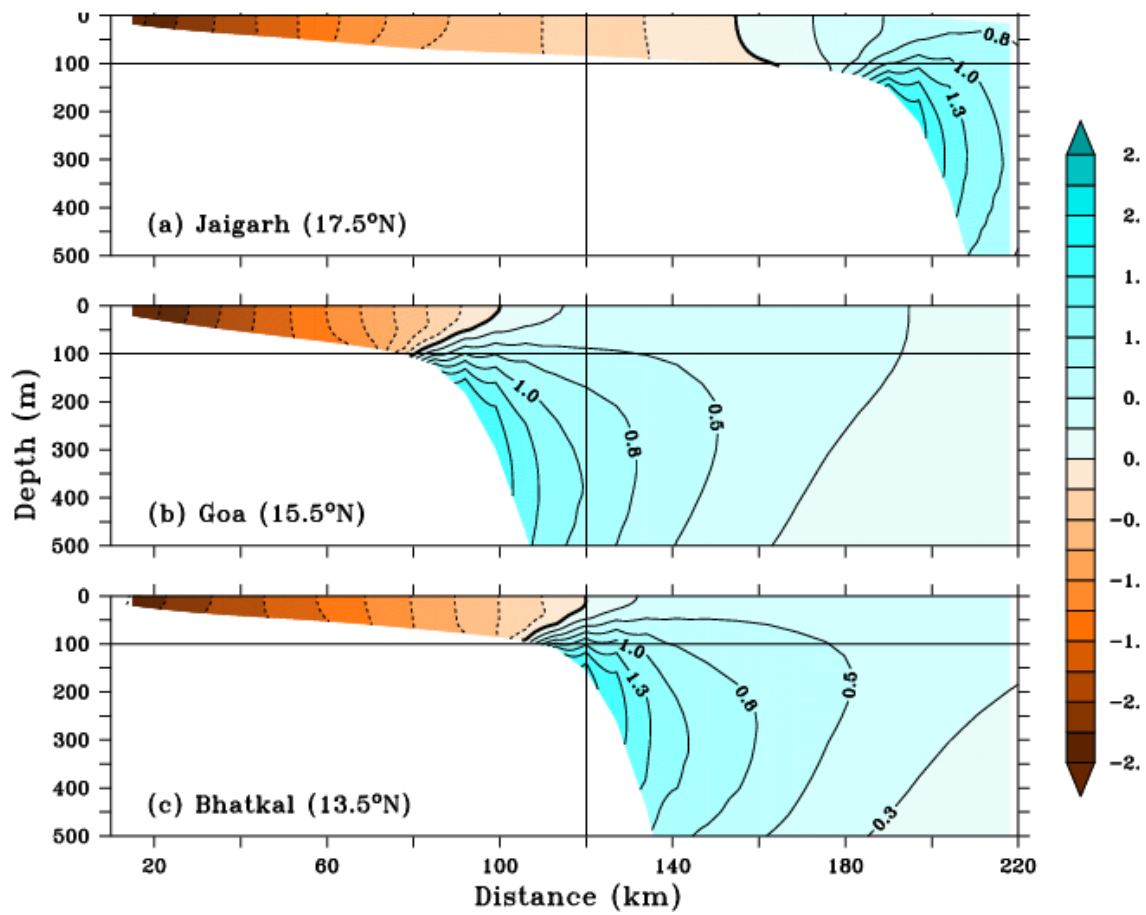


Figure 16: Offshore vertical structure for the second mode alongshore currents at (a) Jaigarh, (b) Goa, and (c) Bhatkal. The units are arbitrary, and only the top 500 m is shown. The thick contour is the zero contour. The horizontal line marks the 100 m water-column depth and the vertical line marks the 120 km distance away from the coast.

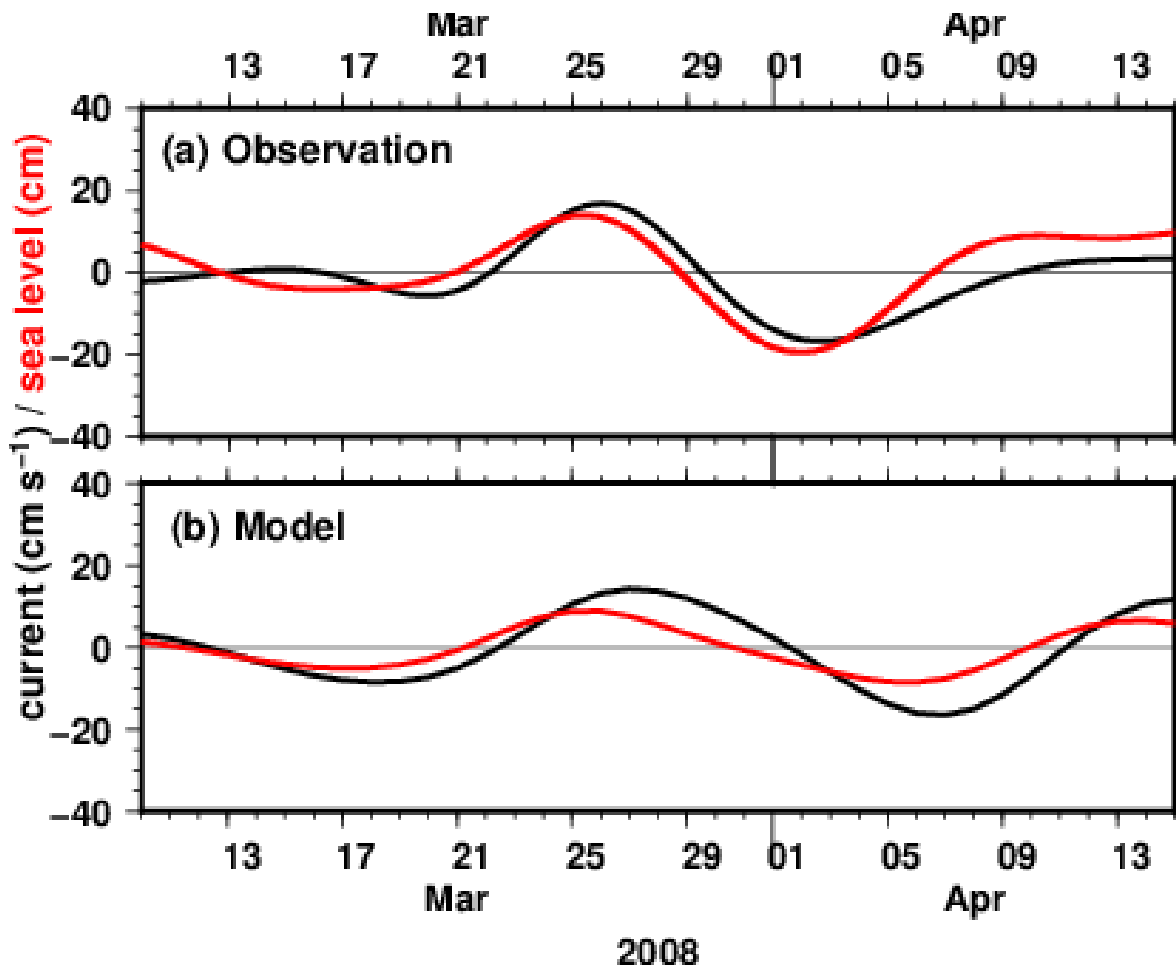


Figure 17: 10–30-day band-passed current (black) and sea level (red) from (a) observations and (b) CTW model. The sea level is scaled (3 times) to highlight the phase difference between the current. The results from CTW model are shown after summation of first three modes.

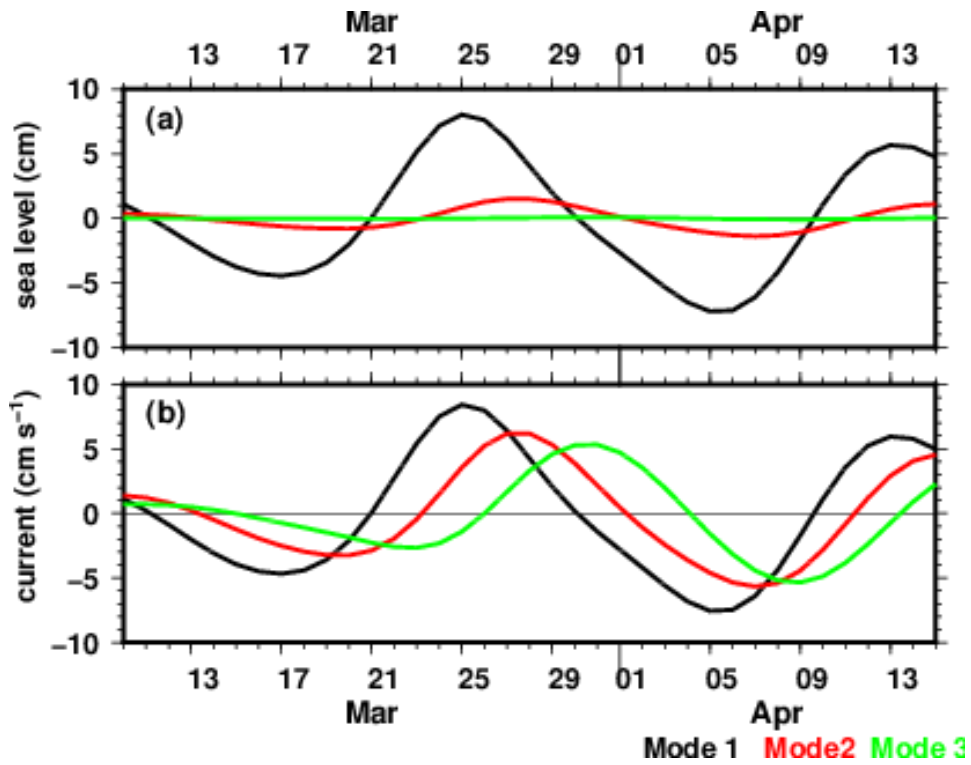


Figure 18: 10–30-day band-passed (a) sea level and (b) current from CTW model for first (black), second (red), and third (green) mode. The model is forced with QuikSCAT winds. The sea level is scaled by a factor of 3.